frontiers

Supplementary Material

Contents of this file

Supplementary Text 1, Supplementary Figures 1–7, Supplementary Tables 1–10, and References

Supplementary Text 1. Wave-ice models in WW3

A brief overview of six wave–ice parameterization models, denoted as IC0–IC5 in WW3, and the ice parameters used in this study, are provided here.

IC0 was updated by Tolman (2003) to a "continuous treatment" to allow partial blocking of partial ice cover. In this method, a user defines two critical ice concentrations that describe the minimum concentration that affects the waves ($C_{\mathrm{i,0}}$), and the concentration at which the wave energy is completely blocked ($C_{\mathrm{i,n}}$). For the ice concentration between $C_{\mathrm{i,0}}$ and $C_{\mathrm{i,n}}$, the wave energy is partially blocked or transmitted based on linear interpolation between the two values. In the present study, these critical ice concentrations are $C_{\mathrm{i,0}}$= 0.25, and $C_{\mathrm{i,n}}$= 0.75. IC0 does not treat the effect as "dissipation" via the S_{ice} source function, but rather as a feature of the propagation schemes. In addition, this method does not permit variation in the dissipation rate with frequency. The details of IC0 can be found in Tolman (2003).

IC1 is the first S_{ice} source function in WW3, based on Rogers and Orzech (2013). In this source term, the user provides the exponential attenuation rate (k_{i}) of the wave amplitude with distance. The attenuation rate did not vary with the frequency space. In the present study, $k_{\mathrm{i}} = 2 \times 10^{-5}$ is used.

IC2 is based on the method proposed by Liu and Mollo-Christensen (1988). This model is derived based on the assumption that dissipation is caused by trbulence in the boundary layer between the ice and the water layer, with the ice modeled as a continuous thin elastic plate. The input parameters are the ice thickness (h_{i}) and kinematic viscosity (ν) in the boundary layer beneath the ice. The dispersion relation of IC2 is defined as:

$$\sigma^2 = \frac{\mathrm{g}k_{\mathrm{r}} + Bk_{\mathrm{r}}^5}{\coth(k_{\mathrm{r}}d) + (k_{\mathrm{r}}M)}, \tag{1}$$

$$C_{\mathrm{g}} = \frac{\mathrm{g} + (5 + 4k_{\mathrm{r}}M)Bk_{\mathrm{r}}^5}{2\sigma(1 + k_{\mathrm{r}}M)^2}, \tag{2}$$

$$\alpha = \frac{\sqrt{\nu\sigma}k_{\mathrm{r}}}{C_{\mathrm{g}}\sqrt{2}(1 + k_{\mathrm{r}}M)}, \tag{3}$$

where g is the gravitational acceleration, and d is the water depth. B and M denote the effects that modify the frequency owing to the bending of the ice and the inertia of the ice, respectively. B and M

depend on the ice thickness (Liu and Mollo-Christensen, 1988; Liu et al., 1991 for details). In the present study, we used the ν values provided by Liu et al. (1991), Li et al. (2015), and Liu et al. (2020a), as shown in **Supplementary Table 1**. Thus, three IC2 simulation cases were performed.

IC3 employs the viscoelastic model proposed by Wang and Shen (2010). IC3 theorizes that ice can store and dissipate energy; thus, the model assumes ice as a viscoelastic layer. The storage property is reflected in the potential and elastic energy, and the dissipative property is equivalent to viscous damping. The dispersion relation of IC3 can be described as:

$$\sigma^2 - Qgk\tanh(kd) = 0, \tag{4}$$

$$Q = 1 + \frac{\rho_{\mathrm{i}}}{\rho_{\mathrm{w}}}\frac{(\mathrm{g}^2k^2 - K^4 - 16k^6a^2\nu_e^4)S_kS_a - 8k^3a\nu_e^2K^2(C_kC_a - 1)}{\mathrm{g}k(4k^3a\nu_e^2S_kC_a + K^2S_aC_k - \mathrm{g}kS_kS_a)}. \tag{5}$$

In the above, $a^2 = k^2 - i\sigma/\nu_e$, $S_k = sinh(kh_{\mathrm{i}})$, $S_a = sinh(ah_{\mathrm{i}})$, $C_k = cosh(kh_{\mathrm{i}})$, $C_a = cosh(ah_{\mathrm{i}})$, $K = \sigma + 2ik^2\nu_e$, $\nu_e = \nu + iG/\rho_{\mathrm{i}}\sigma$. $\rho_{\mathrm{w}}(\rho_{\mathrm{i}})$ is the density of water (sea ice). ρ_{w} is 1025 kg m^{-3} in this study. The IC3 model requires four ice parameters: ice thickness, kinematic viscosity, ice density, and effective shear modulus (G). In this study, we have implemented values of $\rho_{\mathrm{i}} = 917$ (kg m^{-3}). In the present study, we used the theoretical values (ν and G) following the WW3 manual and previous studies (Li et al. 2015; Rogers et al. 2016; Liu et al. 2020a) (**Supplementary Table 1**). Therefore, four IC3 simulation cases were conducted.

The concept of IC4 is a simple, efficient, and flexible implementation of frequency-or period-dependent wave attenuation. Details of IC4 were introduced by Collins and Rogers (2017). There are seven methods in IC4, denoted as IC4M1–M7, as follows:

IC4M1 has an exponential equation that fits the data of Wadhams et al. (1988). The equation is as follows:

$$\alpha = exp[-C_1T - C_2], \tag{6}$$

where $T = 2\pi/\sigma$ is the wave period. Following Wadhams et al. (1988), we used the following parameters: C_1 = 0.18, C_2 = 7.3.

IC4M2 is polynomial fit depend on frequency (f =1/ T) as follows:

$$\alpha = C_1 + C_2f + C_3f^2 + C_4f^3 + C_5f^4. \tag{7}$$

In this method, the dissipation is represented using a user-specified polynomial. Thus, it is a flexible method as a user has the freedom to change all the coefficients of the polynomial; in this case, it is the shape of the attenuation function. In this study, we used the coefficients (C_3 and C_5) of binomial fitting suggested by Meylan et al. (2014), Rogers et al. (2018), and Rogers et al. (2021) (**Supplementary Table 2**). Thus, eight simulation cases were conducted for IC4M2. IC4M6H1–H3 used the coefficients of the binomial equation fitted to the step functions of IC4M6, as shown in **Supplementary Table 3**. Surface Wave Instrument Float with Tracking (SWIFT) buoy (Thomson 2012), U.K. wave buoy (Wadhams and Thomson 2015), and National Institute of Water and Atmospheric Research (NIWA) buoy (Kohout et al. 2015) from Wave Array 3 (WA3) of the Office of Naval Research (ONR) "Sea State" experiment are used for the parameterizations of IC4M2. See Rogers et al. (2018) for details on

IC4M6H1, IC4M6H2, IC4M6H3, WA3 SWIFT, WA3 UK, and WA3 NIWA in **Supplementary Table 2**.

IC4M3 is based on the work of Horvat and Tziperman (2015). Horvat and Tziperman (2015) fitted a quadratic equation to the attenuation coefficient calculated by Kohout and Meylan (2008), depending on the wave period ($T = 1/f$) and ice thickness (h_i). The attenuation rate increases as the wave period and ice thickness increase. This equation has the following form:

$$\ln \alpha = -0.3203 + 2.058h_\mathrm{i} - 0.9375T - 0.4269h_\mathrm{i}^2 + 0.1566h_\mathrm{i}T + 0.0006T^2. \quad (8)$$

Attenuation of IC4M4 is a function of the significant wave height (H_s) (Kohout et al. 2014):

$$\frac{dH_s}{dx} = \begin{cases} C_1 \times H_s & \text{for } H_s \leq 3\ m \\ C_2 & \text{for } H_s > 3\ m' \end{cases} \quad (9)$$

here, $k_\mathrm{i} = dH_s/dx$. The attenuation rate increases linearly with H_s until H_s= 3 m, regardless of the frequency. Following Kohout et al. (2014), 5.35 × 10^{-6} and 16.05 × 10^{-6} are used for C_1 and C_2, respectively.

IC4M5 provides attenuation as a step function in the frequency space in four steps. This method is provided by nonstationary and nonuniform parameters ($C_1 - C_7$). $C_1 - C_4$ determines the values of attenuation (k_i) at each step, and $C_5 - C_7$ controls the end of the frequency range (given in Hz) of the first three steps. However, this method was not used in this study because IC4M5 cannot set the step function more finely than IC4M6, as shown below.

IC4M6 is also a step function similar to IC4M5, but has a frequency space of 10 steps. Furthermore, it is a spatiotemporally constant step function. In this method, such as IC4M5, a user defines the attenuation rate (k_i) at each step and the end of the frequency range (in Hz). In the present study, six simulation cases were performed, as shown in **Supplementary Table 3**. The values in **Supplementary Table 3** are the parameters proposed by Rogers et al. (2018). "WA3 Doble" in **Supplementary Table 3** is based on the data of Doble et al. (2015).

IC4M7 uses the monomial expression for dissipation by Doble et al. (2015). Similarly, for IC4M3, the equation depends on wave period (T) and ice thickness (h_i):

$$\alpha = 0.2T^{-2.13}h_\mathrm{i}. \quad (10)$$

IC5 is based on a viscoelastic beam model of Mosig et al. (2015). Relation of Eq. (4) is the same as IC3, while estimation of Q is different as follow:

$$Q = \frac{G_\nu h_\mathrm{i}^3}{6\rho_\mathrm{w}\mathrm{g}}(1+V)k^4 - \frac{\rho_\mathrm{i}h_\mathrm{i}\sigma^2}{\rho_\mathrm{w}\mathrm{g}} + 1, \quad (11)$$

where $G_\nu = G - i\sigma\rho_\mathrm{i}\nu$ is the complex shear modulus, and V is the Poisson's ratio (0.3) of ice. IC5 is also a viscoelastic model, similar to IC3. However, IC3 is an extension of the viscous ice layer model with a finite thickness (Keller, 1998), which includes elasticity into a complex viscosity (Wang and Shen, 2010). In contrast, IC5 is an extension of the thin elastic plate model (Fox and Squire, 1994) introduced by Mosig et al. (2015) by adding viscosity to a complex shear modulus. Similar to IC3, the input parameters of IC5 are ice thickness, kinematic viscosity, ice density, and effective shear modulus.

The parameters used were as follows: ρ_i = 917 (kg m^{-3}). Two IC5 simulation cases were conducted, using the theoretical values (ν and G) suggested by Mosig et al. (2015) and Liu et al. (2020b) (**Supplementary Table 1**).

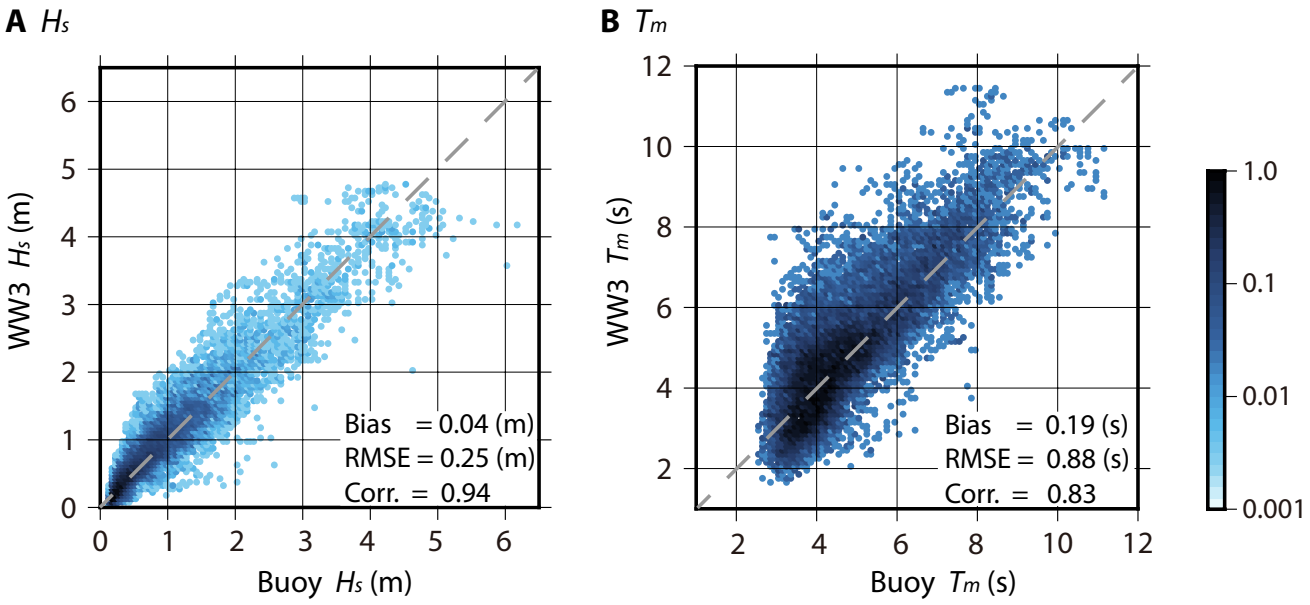

Supplementary Figure 1. Same as **Figure 3** but with model results with ST4.

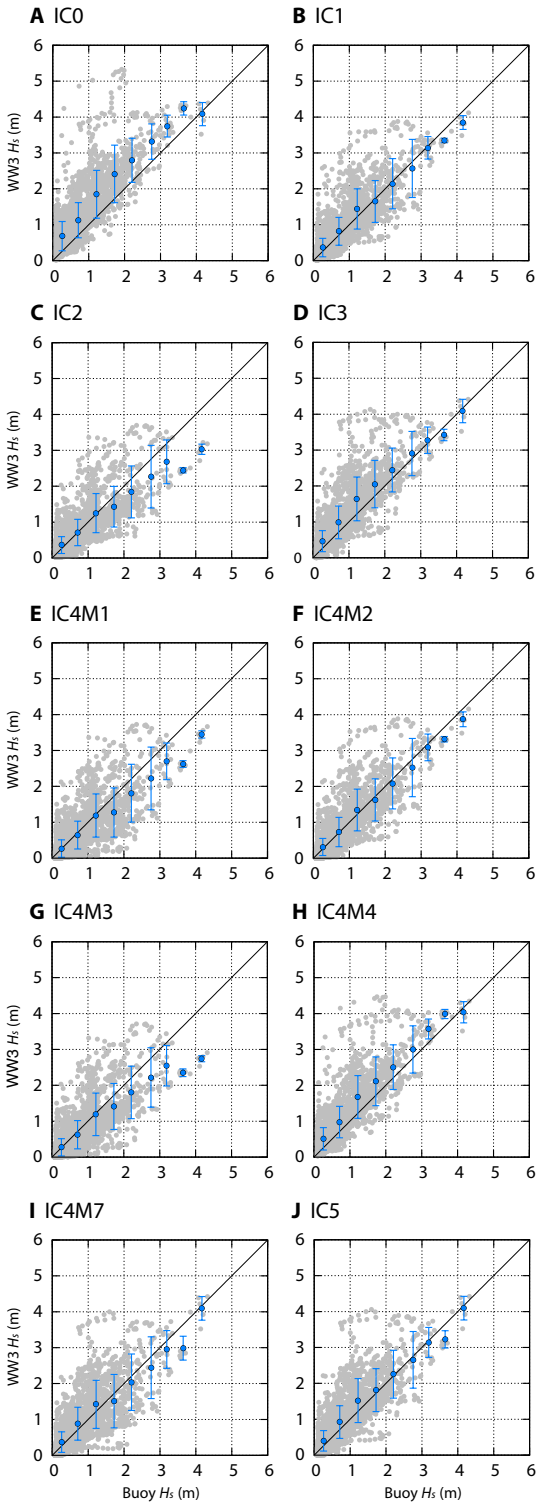

Supplementary Figure 2. Scatter diagrams of H_s between the ST6 model simulation (y–axis) versus buoy observation (x–axis) for the ice-covered condition. Light blue circles represent the model simulation values within each bin of the buoy observation at intervals of 0.5 m, and the error bars represent the RMSE in each bin. Gray circles show the hourly model simulations and buoy observation. The number of validation data points is 3277.

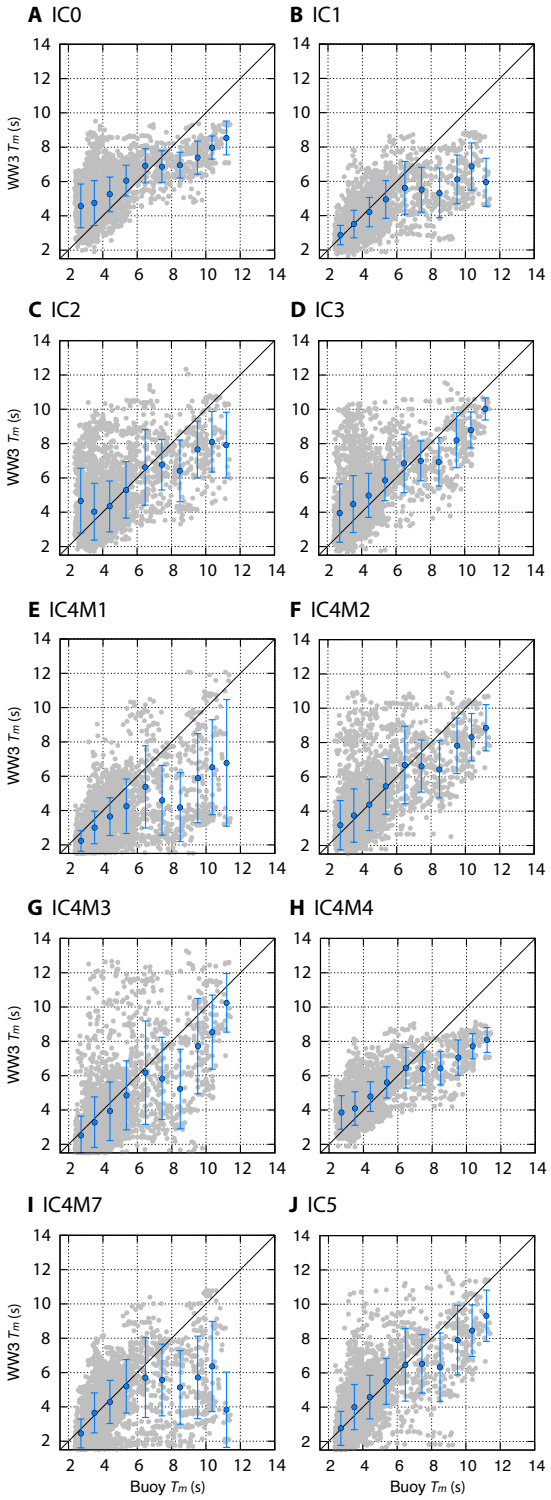

Supplementary Figure 3. Same as **Supplementary Figure 2** but for T_m. Light blue circles indicate the model simulation values within each bin of the buoy observation at intervals of 1 s.

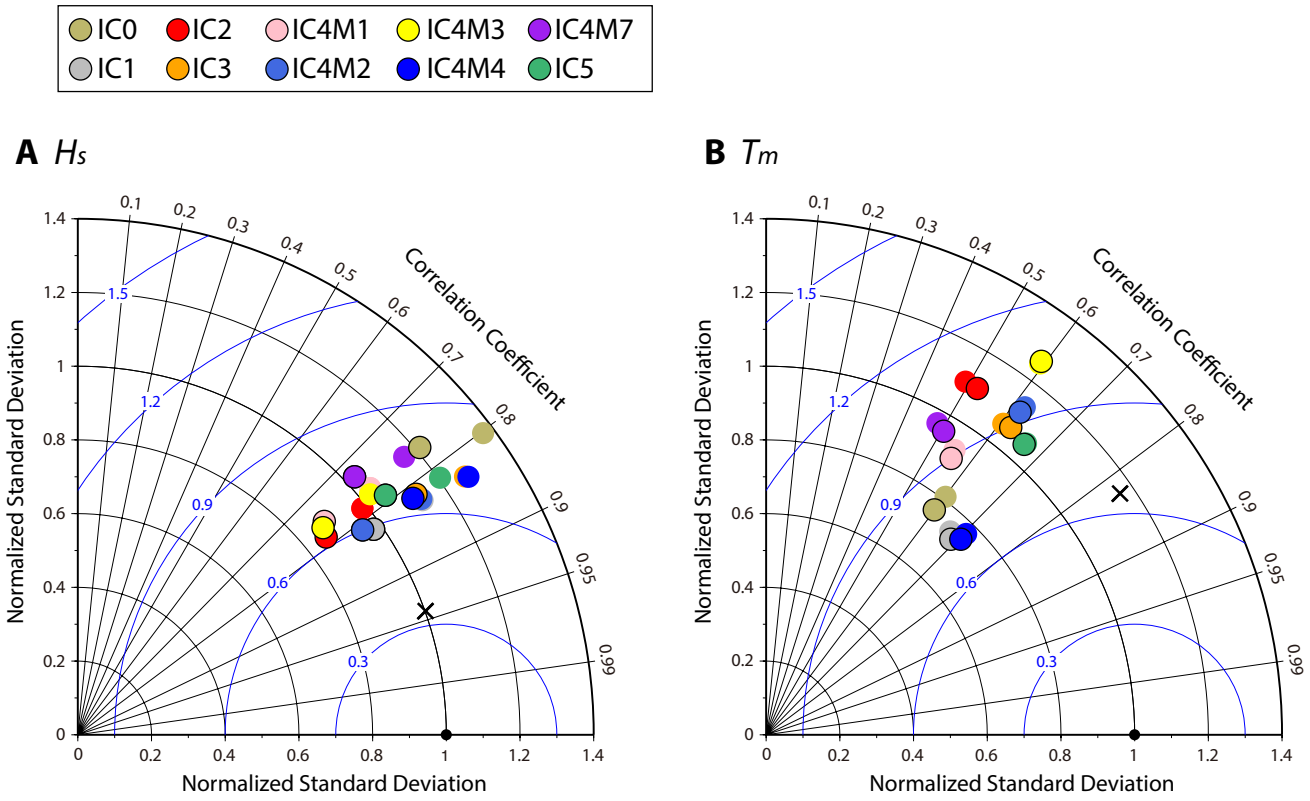

Supplementary Figure 4. Same as **Figure 4** but with model results with ST4 (markers with black outlines). ST6 simulations (markers without black outlines) in **Figure 4** also shown in both figures.

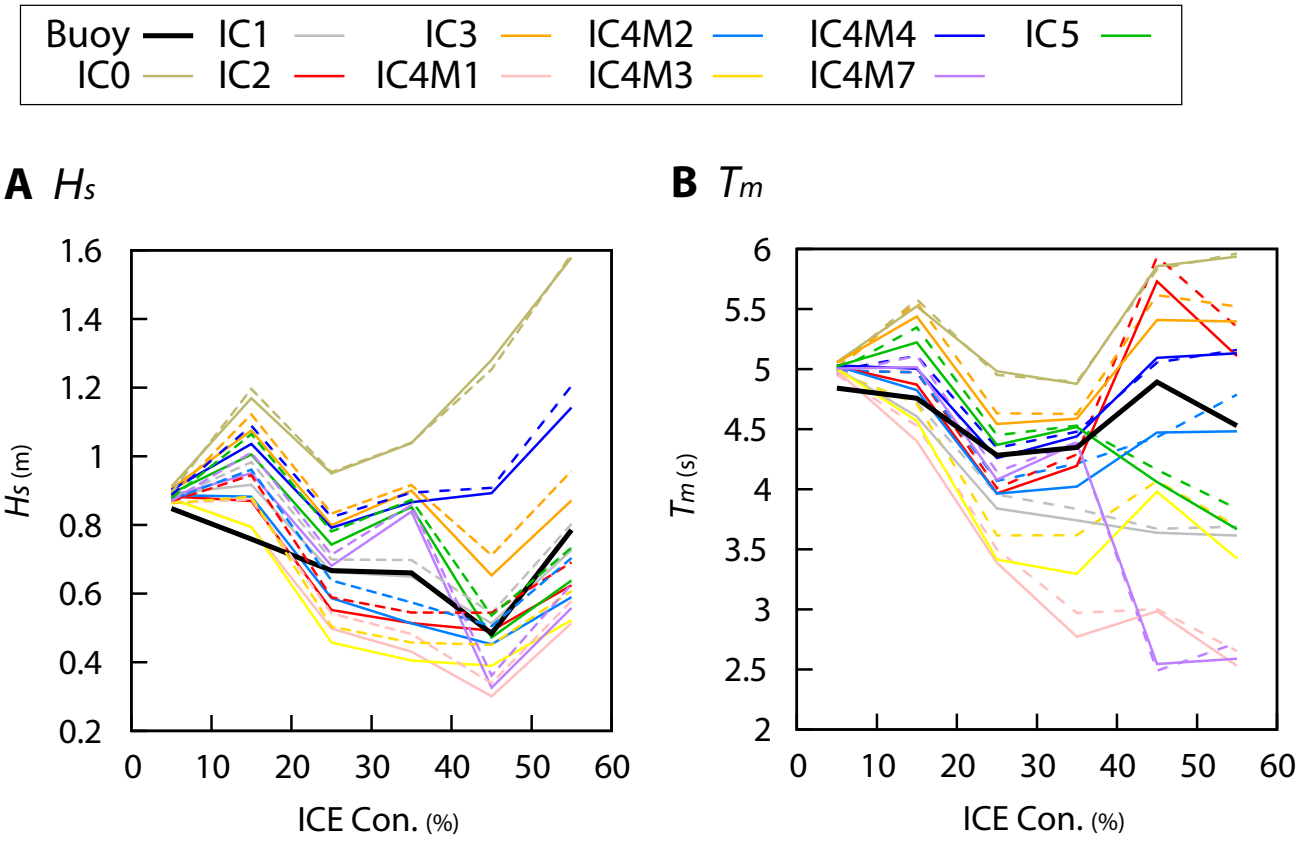

Supplementary Figure 5. Same as **Figure 5** but for model results with ST4 (colored lines). ST6 simulations (broken colored lines) in **Figure 5** also indicated in both figures.

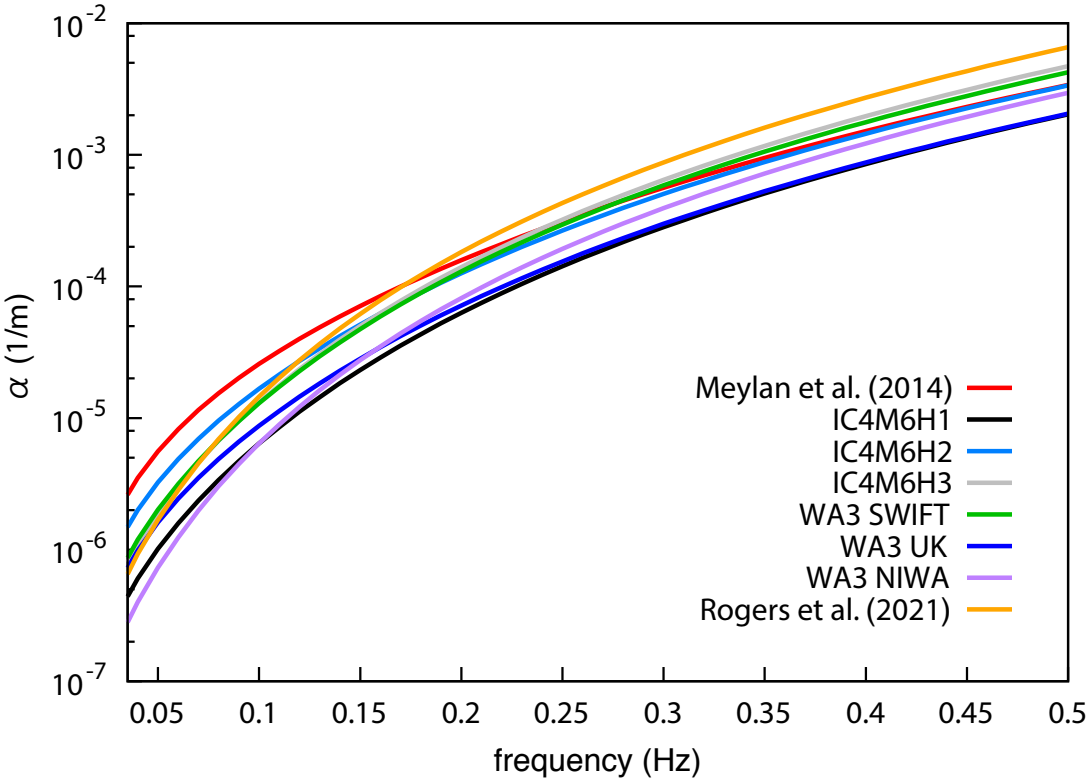

Supplementary Figure 6. Attenuation rate (α) as a function of frequency for eight binomial functions of IC4M2 employed in this study. The line colors are defined in the legend in the lower right corner.

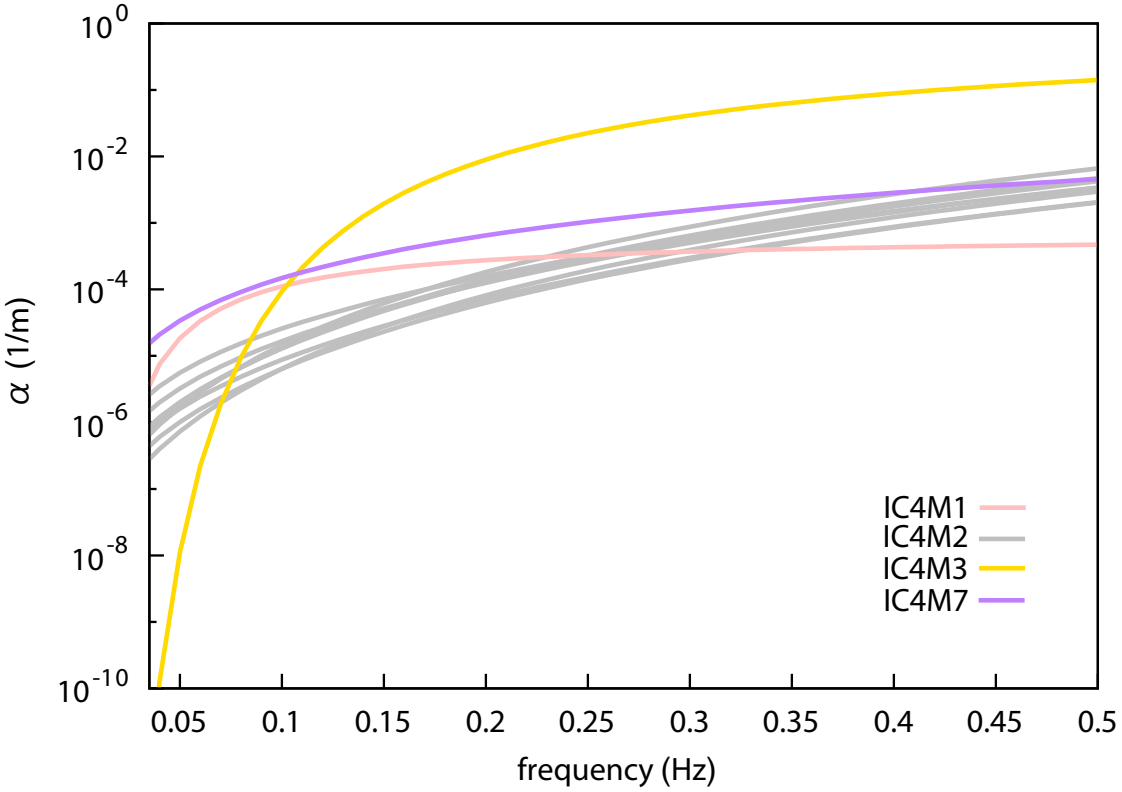

Supplementary Figure 7. Attenuation rate (α) as a function of frequency for four binomial functions of IC4M1, IC4M2, IC4M3, and IC4M7 employed in this study. The line colors are defined in the legend in the lower right corner. In this figure, h_i = 5 cm is used for IC4M3 and IC4M7. Gray lines show the eight binomial functions of IC4M2 in **Supplementary Figure 6**.

Supplementary Table 1. Theoretical parameters (ν and G) for IC2, IC3, and IC5 used in this study.

Model	ν ($m^2 s^{-1}$)	G (Pa)	Reference
IC2			
	1.536×10^{-1}	–	Liu et al. (1991)
	1.0×10^{-5}	–	Li et al. (2015)
	7.5683×10^{-5}	–	Liu et al. (2020a)
IC3			
	1.0	1.0×10^{3}	WW3 manual
	0.2	2.0×10^{4}	Li et al. (2015)
	0.03	0	Rogers et al. (2016)
	0.328	3.1318×10^{4}	Liu et al. (2020a)
IC5			
	5.0×10^{7}	4.9×10^{12}	Mosig et al. (2015)
	1.6×10^{7}	4.0×10^{12}	Liu et al. (2020b)

Supplementary Table 2. Values of C_3 and C_5 for IC4M2 used in this study.

Name	C_3	C_5
Meylan et al. (2014)	2.120e-03	4.590e-02
IC4M6H1	3.280e-04	3.120e-02
IC4M6H2	1.176e-03	4.920e-02
IC4M6H3	5.800e-04	7.320e-02
WA3 SWIFT	6.420e-04	6.520e-02
WA3 UK	5.680e-04	3.060e-02
WA3 NIWA	1.758e-04	4.660e-02
Rogers et al. (2021)	4.160e-04	1.036e-01

Supplementary Table 3. k_{i} values for each frequency range of IC4M6 used in this study.

Frequency range (Hz)	IC4M6H1	IC4M6H2	IC4M6H3	WA3 SWIFT	WA3 Doble	WA3 NIWA
			k_{i} (1/m)			
0.035-0.045	1.00e-06	1.00e-06	1.00e-06	1.00e-06	1.00e-06	1.00e-06
0.045-0.055	2.00e-06	2.00e-06	2.00e-06	2.00e-06	2.00e-06	2.00e-06
0.055-0.100	2.94e-06	5.10e-06	4.22e-06	4.48e-06	4.92e-06	2.13e-06
0.100-0.150	4.27e-06	1.50e-05	1.24e-05	1.12e-05	5.80e-06	3.86e-06
0.150-0.200	7.95e-06	3.00e-05	2.26e-05	2.28e-05	8.62e-06	1.46e-05
0.200-0.250	2.95e-05	6.40e-05	6.92e-05	6.91e-05	3.28e-05	5.47e-05
0.250-0.300	1.12e-04	1.50e-04	2.24e-04	2.06e-04	9.70e-05	1.59e-04
0.300-0.350	2.74e-04	3.40e-04	5.80e-04	5.08e-04	2.59e-04	3.25e-04
0.350-0.400	4.95e-04	7.50e-04	1.10e-03	9.33e-04	5.51e-04	5.68e-04
0.400-1.100	8.94e-04	1.40e-03	1.94e-03	1.69e-03	1.00e-03	1.32e-03

Supplementary Table 4. Statistical values of H_s and T_m between buoy observation and IC2 simulations with ST6. In this comparison, based on 3277 validation data point, we used the values for the ice-covered condition.

	Liu et al. (1991)	Li et al. (2015)	Liu et al. (2020a)
H_s			
Bias (m)	0.01	0.01	0.02
RMSE (m)	0.41	0.41	0.41
Corr.	0.78	0.78	0.78
T_m			
Bias (s)	0.22	0.21	0.21
RMSE (s)	1.89	1.91	1.88
Corr.	0.49	0.49	0.5

Supplementary Table 5. Same as **Supplementary Table 4** but for IC3 simulations with ST6.

	WW3 manual	Li et al. (2015)	Rogers et al. (2016)	Liu et al. (2020a)
H_s				
Bias (m)	0.27	0.29	0.45	0.25
RMSE (m)	0.44	0.45	0.51	0.44
Corr.	0.83	0.83	0.81	0.83
T_m				
Bias (s)	0.81	0.89	1.21	0.6
RMSE (s)	1.73	1.77	1.7	1.63
Corr.	0.57	0.56	0.5	0.61

Supplementary Table 6. Same as **Supplementary Table 4** but for IC5 simulations with ST6.

	Mosig et al. (2015)	Liu et al. (2020b)
H_s		
Bias (m)	0.17	0.24
RMSE (m)	0.43	0.44
Corr.	0.82	0.83
T_m		
Bias (s)	0.09	0.47
RMSE (s)	1.5	1.51
Corr.	0.67	0.65

Supplementary Table 7. Same as **Supplementary Table 4** but for IC4M2 simulations with ST6.

	Meylan et al. (2014)	IC4M6H1	IC4M6H2	IC4M6H3	WA3 SWIFT	WA3 UK	WA3 NIWA	Rogers et al. (2021)
H_s								
Bias (m)	0.03	0.20	0.08	0.10	0.10	0.17	0.18	0.07
RMSE (m)	0.40	0.44	0.40	0.41	0.41	0.42	0.44	0.41
Corr.	0.82	0.84	0.83	0.83	0.84	0.84	0.83	0.83
T_m								
Bias (s)	-0.02	0.78	0.28	0.41	0.42	0.64	0.77	0.34
RMSE (s)	1.67	1.78	1.72	1.77	1.76	1.75	1.81	1.78
Corr.	0.62	0.54	0.6	0.58	0.58	0.56	0.54	0.59

Supplementary Table 8. Same as **Supplementary Table 4** but for IC4M6 simulations with ST6.

	IC4M6H1	IC4M6H2	IC4M6H3	WA3 SWIFT	WA3 Doble	WA3 NIWA
H_s						
Bias (m)	0.24	0.10	0.12	0.12	0.20	0.23
RMSE (m)	0.44	0.40	0.41	0.41	0.42	0.45
Corr.	0.83	0.84	0.84	0.84	0.84	0.83
T_m						
Bias (s)	0.77	0.33	0.44	0.45	0.59	0.87
RMSE (s)	1.66	1.69	1.7	1.69	1.62	1.75
Corr.	0.56	0.59	0.59	0.58	0.57	0.53

Supplementary Table 9. Same as **Table 1** but for the statistical values of daily data. We used 146 daily validation data points.

	IC0	IC1	IC2	IC3	IC4M1	IC4M2	IC4M3	IC4M4	IC4M7	IC5
H_s										
Bias (m)	0.47	0.1	**0.02**	0.26	-0.06	**0.04**	**-0.05**	0.3	0.1	0.17
RMSE (m)	0.47	**0.33**	**0.35**	0.39	0.37	**0.34**	0.37	0.39	0.43	0.38
Corr.	0.82	**0.85**	0.8	**0.85**	0.78	0.84	0.79	**0.85**	0.77	0.83
T_m										
Bias (s)	0.78	-0.44	**0.22**	0.6	-0.99	**-0.03**	-0.5	0.25	-0.44	**0.06**
RMSE (s)	1.17	**1.04**	1.48	1.32	1.29	1.23	1.28	**0.97**	1.51	**1.09**
Corr.	0.7	**0.76**	0.59	0.68	0.64	0.73	0.73	**0.8**	0.55	**0.78**

Supplementary Table 10. Same as **Table 1** but for the model simulations with ST4.

	IC0	IC1	IC2	IC3	IC4M1	IC4M2	IC4M3	IC4M4	IC4M7	IC5
H_s										
Bias (m)	0.46	**0.04**	**-0.04**	0.21	-0.13	**-0.04**	-0.13	0.25	0.05	0.11
RMSE (m)	0.49	**0.37**	**0.39**	0.41	0.41	**0.37**	0.41	0.4	0.46	0.42
Corr.	0.77	**0.82**	0.78	**0.81**	0.76	**0.81**	0.76	**0.82**	0.73	0.79
T_m										
Bias (s)	0.8	-0.53	**0.1**	0.5	-1.1	**-0.17**	-0.71	0.2	-0.46	**-0.01**
RMSE (s)	**1.46**	**1.3**	1.84	1.6	1.6	1.65	1.86	**1.27**	1.73	1.5
Corr.	0.6	**0.69**	0.52	0.62	0.56	0.62	0.59	**0.71**	0.51	**0.66**

References

Doble, M. J., Carolis, G. Ge., Meylan, M. H., Bidlot, J.-R., and Wadhams, P. (2015). Relating wave attenuation to pancake ice thickness, using field measurements and model results, *Geophysical Research Letters,* 42, 4473–4481, doi:10.1002/2015GL063628

Fox, C., and Squire, V. A. (1994). On the oblique reflexion and transmission of ocean waves at shore fast sea ice. *Philosophical Transactions of the Royal Society of London Series A*, 347, 185– 218. https://doi.org/10.1098/rsta.1994.0044

Horvat, C., and Tziperman, E. (2015). A prognostic model of sea-ice floe size and thickness distribution. *Cryosphere*, 9, 2119–4134.

Keller, J. B., (1998). Gravity waves on ice-covered water. *Journal of Geophysical Research,* 103, 7663–7669.

Kohout, A. L., and Meylan, M. H. (2008). An elastic plate model for wave attenuation and ice floe breaking in the marginal ice zone. *Journal of Geophysical Research*, 113, (C9), doi:10.1029/2007JC004434

Kohout, A. L., Penrose, B., Penrose, S., and Williams, M.J.M. (2015). A device for measuring wave-induced motion of ice floes in the Antarctic marginal ice zone. *Annals of Glaciology*, 56 (69), 415–424.

Li, J., Kouhout, A. L., and Shen, H. H. (2015). Comparison of wave propagation through ice covers in calm and storm conditions. *Geophysical Research Letters,* 42, 5935–5941, doi:10.1002/2015GL064715

Liu, D., Tsarau, A., Guan, C., and Shen, H. H. (2020a). Comparison of ice and wind-wave in in WAVEWATCH III ® in the Barents sea, *Cold Regions and Science Technology*. 172, https://doi.org/10.1016/j.coldregions.2020.103008

Liu, Q., Rogers, W. E., Babanin, A., Li, J., and Guan, C. (2020b). Spectral modeling of ice-induced wave decay. *Journal of Physical Oceanography*, 50(6), 1583–1604. https://doi.org/10.1175/JPO-D-19-0187.1

Rogers, W. E., Thomson, J., Shen, H. H., Doble, M. J., Wadhams, P., and Cheng, S. (2016). Dissipation of wind waves by pancake and frazil ice in the autumn Beaufort Sea. *Journal of Geophysical Research*. 121, 7991–8007, https://doi.org/10.1002/2016/JC012251

Rogers, W. E., Meylan, M. H., and Kohout, A. L. (2018). Frequency distribution of dissipation of energy of ocean waves by sea ice using data from Wave Array 3 of the ONR "Sea State" field experiment, (Technical Memo. NRL/MR7322–18-9801) Naval Research Laboratory.

Rogers, W. E., Meylan, M. H., and Kohout, A. L. (2021). Estimates of spectral wave attenuation in Antarctic sea ice using mode/data inversion. *Cold Regions Science and Technology,* 182, https://doi.org/10.1016/j.coldregions.2020.103198

Thomson, J. (2012). Wave breaking dissipation observed with SWIFT drifters. *Journal of Atmospheric and Oceanic Technology,* 29, 1866–1882, doi:10.1175/JTECH-D-12-00018.1

Wadhams, P. and J. Thomson. (2015). The Arctic Ocean cruise of R/V Sikuliaq 2015, An investigation of waves and the advancing ice edge. *II Polo*, 70(4), 9–38.

Wadhams, P., V. A. Squire, D. J. Goodman, A. M. Cowan, and S. C. Moore (1988). The attenuation rates of ocean waves in the marginal ice zone, *Journal of Geophysical Research,* 93, 6799–6818.